ResearchGate

See discussions, stats, and author profiles for this publication at: https://www.researchgate.net/publication/228667477

The effective-field study of a mixed spin-1 and spin-5/2 Ising ferrimagnetic system

Article *in* Physica Scripta · June 2009

DOI: 10.1088/0031-8949/79/06/065006

CITATIONS
28

READS
457

3 authors:

Bayram Deviren
Nevşehir Hacı Bektaş Veli University
67 PUBLICATIONS **1,774** CITATIONS
SEE PROFILE

Mehmet Bati
Recep Tayyip Erdoğan Üniversitesi
29 PUBLICATIONS **169** CITATIONS
SEE PROFILE

Mustafa Keskin
Erciyes Üniversitesi
245 PUBLICATIONS **5,173** CITATIONS
SEE PROFILE

All content following this page was uploaded by Bayram Deviren on 22 May 2014.

The user has requested enhancement of the downloaded file.

IOPscience iopscience.iop.org

Home Search Collections Journals About Contact us My IOPscience

The effective-field study of a mixed spin-1 and spin-5/2 Ising ferrimagnetic system

This article has been downloaded from IOPscience. Please scroll down to see the full text article.

2009 Phys. Scr. 79 065006

(http://iopscience.iop.org/1402-4896/79/6/065006)

View the table of contents for this issue, or go to the journal homepage for more

Download details:
IP Address: 95.183.152.38
The article was downloaded on 16/03/2011 at 11:30

Please note that terms and conditions apply.

Phys. Scr. **79** (2009) 065006 (11pp) doi:10.1088/0031-8949/79/06/065006

The effective-field study of a mixed spin-1 and spin-5/2 Ising ferrimagnetic system

Bayram Deviren[1,2], **Mehmet Batı**[1,3] **and Mustafa Keskin**[4]

[1] Institute of Science, Erciyes University, 38039 Kayseri, Turkey
[2] Department of Physics, Nevsehir University, 50300 Nevsehir, Turkey
[3] Department of Physics, Rize University, 53100 Rize, Turkey
[4] Department of Physics, Erciyes University, 38039 Kayseri, Turkey

E-mail: keskin@erciyes.edu.tr

Received 14 November 2008
Accepted for publication 6 April 2009
Published 22 May 2009
Online at stacks.iop.org/PhysScr/79/065006

Abstract
An effective-field theory with correlations is developed for a mixed spin-1 and spin-5/2 Ising ferrimagnetic system on the honeycomb ($\delta = 3$) and square ($\delta = 4$) lattices in the absence and presence of a longitudinal magnetic field. The ground-state phase diagram of the model is obtained in the longitudinal magnetic field (h) and a single-ion potential or crystal-field interaction (Δ) plane. We also investigate the thermal variations of the sublattice magnetizations, and present the phase diagrams in the ($\Delta/|J|, k_B T/|J|$) plane. The susceptibility, internal energy and specific heat of the system are numerically examined, and some interesting phenomena in these quantities are found due to the absence and presence of the applied longitudinal magnetic field. Moreover, the system undergoes second- and first-order phase transition; hence, the system gives a tricritical point. The system also exhibits reentrant behavior.

PACS numbers: 05.50.+q, 05.70.Fh, 75.10.Hk, 75.30.Kz, 75.50.Gg

1. Introduction

During the past several decades, much effort has been devoted to determine the critical behavior and other statistical properties of the various Ising systems, which would enable a deeper understanding of order–disorder phenomena in statistical physics and condensed matter physics. The Ising systems consisting of mixed spins of different magnitudes, the so-called mixed-spin Ising models, are among the most interesting extensions of the standard spin-1/2 Ising system. Mixed spin Ising systems provide good models to investigate ferrimagnetic materials that are currently of great interest due to their possible useful properties for technological applications, as well as academic research. The well-known mixed spin Ising systems are spins (1/2, 1), spins (1/2, 3/2) and spins (1, 3/2) Ising systems. These systems have been studied extensively by using the methods of equilibrium statistical physics such as the mean-field approximation (MFA), effective-field theory (EFT), cluster variation method (CVM), renormalization group (RG) techniques and Monte-Carlo (MC) simulations (see [1–5] for spins (1, 1/2), [6–10] for spins (1/2, 3/2) and [11–15] for spins (1, 3/2) Ising systems, and references therein). Moreover, the exact solutions of the spins (1/2, 1) were studied on a honeycomb lattice [16], a bathroom tile [17], diced lattices [18], a Bethe lattice [19], a two-fold Cayley tree [20], several decorated planar lattices [21] and a bilayer Bethe lattice [22]. Dynamics of the mixed spin-1/2 and spin-1 Ising system [23, 24] has also been investigated by using the Glauber-type stochastic dynamics [25], the dynamical pair approximation [26], the dynamic MC simulations and finite-size scaling arguments [27], the MC simulations and the dynamical pair approximation [28, 29] and the pair approximation with point distribution [30]. The exact solution of spins (1/2, 3/2) Ising system has also been studied on the Bethe lattice [31] and a two-fold Cayley tree [32] by using the exact recursion relations, on the honeycomb lattice within the framework of exact star–triangle mapping transformations [33], on the extended Kagomé lattice [34] and Union Jack (centered square) lattice [35] by establishing a mapping correspondence with the eight-vertex model. On the other hand, the exact formulation of the mixed spin (1, 3/2) Ising ferrimagnetic system on the Bethe lattice has been examined by using the exact recursion relations [36]. Moreover, recently, the dynamic phase transitions in the kinetic mixed spins (1/2, 3/2) [37] and spins (1, 3/2) [38]

 © 2009 The Royal Swedish Academy of Sciences Printed in the UK

ferrimagnetic systems under a time-dependent magnetic field have been studied by using the Glauber-type stochastic dynamics. The mixed spins (1/2, 5/2) [39–41], spins (3/2, 5/2) [42–44], spins (1, 2) [45–47] and spins (2, 5/2) [48–50] have received less attention. But, up to now, as far as we know, nobody has studied the spin-1 and spin-5/2 Ising system.

Therefore, the aim of this paper is to study the magnetic properties of the mixed spin-1 and spin-5/2 Ising ferrimagnetic system in the absence and presence of a longitudinal magnetic field on the honeycomb and square lattices by using the EFT with correlations in detail. The ground state phase diagram of the model is obtained in the longitudinal magnetic field (h) and a single-ion potential or crystal-field interaction (Δ) plane. We also investigate the thermal variations of the sublattice magnetizations and present the phase diagrams in the $(\Delta/|J|, k_{\mathrm{B}}T/|J|)$ plane for $h = 0$. Moreover, the susceptibility, internal energy and specific heat of the system are numerically examined, and some interesting phenomena in these quantities are found due to the applied longitudinal magnetic field. This method, namely EFT with correlation, was first introduced by Honmura and Kaneyoshi [51] and Kaneyoshi *et al* [52], which is a more advanced method dealing with Ising systems than the MFA, because it considers more correlations. Then, the method has been widely developed and applied to various magnetic systems [53], including thin films, superlattices [54–56] and mixed spin Ising systems [57–59].

The rest of the paper is organized as follows. In section 2, we introduce briefly the basic framework of the EFT with correlations and give the formulation for the mixed spin-1 and spin-5/2 Ising model on the honeycomb and square lattices. In section 3, the numerical results for the magnetizations, phase diagrams and thermodynamic quantities, such as susceptibility, internal energy and specific heat of the model, are studied in detail. The paper ends with a brief summary and conclusion of the work in section 4.

2. Formulation

The mixed spin Ising model on the honeycomb and square lattices is shown in figures 1(a) and (b), respectively. We consider a mixed spin-1 and spin-5/2 Ising model consisting of two sublattices A and B, which are arranged alternately. In the underlying lattice the sites of sublattice A are occupied by spins σ_i, which takes the spin values ± 1, 0, while those of the sublattice B are occupied by spins S_j, which take the spin values $\pm 5/2$, $\pm 3/2$ and $\pm 1/2$. The Hamiltonian of the system is given by

$$H = -J\sum_{\langle ij\rangle}\sigma_i S_j - \Delta\left[\sum_i (\sigma_i)^2 + \sum_j (S_j)^2\right] - h\left[\sum_i \sigma_i + \sum_j S_j\right], \tag{1}$$

where $\langle ij\rangle$ indicates a summation over all pairs of nearest-neighboring sites. J is the bilinear nearest-neighbor exchange interaction, Δ is the crystal-field interaction or single-ion anisotropy and h represents the longitudinal magnetic field.

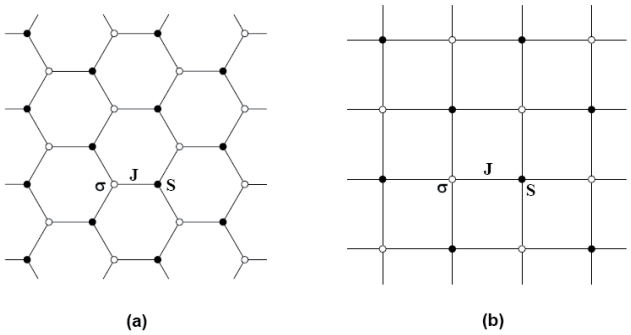

Figure 1. The sketch of the spin arrangement on the honeycomb and square lattices. The open (○) and closed (●) circles denote the spins of $\sigma_i = 1$ and $S_j = 5/2$, respectively. (a) For honeycomb lattice with $\delta = 3$ and (b) for square lattice with $\delta = 4$.

The problem is now the evaluation of the mean values $\langle\sigma_i\rangle$ and $\langle S_j\rangle$. The starting point for statistics of the present spin system is the exact relation due to Callen [60]. As discussed in [57, 61, 62], for the evaluation of mean values $\langle\sigma_i\rangle$ and $\langle S_j\rangle$ we can use the exact Ising spin identities and the differential operator technique introduced by Honmura and Kaneyoshi [51]. Within the framework of the EFT, one finds that

$$\langle(\sigma_i)^k\rangle = \left\langle \prod_\delta \left[A(a) + B(a)S_{j+\delta} + C(a)(S_{j+\delta})^2 + D(a)(S_{j+\delta})^3 + E(a)(S_{j+\delta})^4 + F(a)(S_{j+\delta})^5\right]\right\rangle f_k(x)|_{x=0}, \tag{2}$$

$$\langle(S_j)^k\rangle = \left\langle \prod_\delta \{1 + (\sigma_{i+\delta})\ \sinh(J\nabla) + (\sigma_{i+\delta})^2[\cosh(J\nabla) - 1]\}\right\rangle g_k(x)|_{x=0}, \tag{3}$$

where $a = J\nabla$ and δ denotes the nearest-neighbor sites of the central site i (or a site j); $\nabla = \partial/\partial x$ is a differential operator, and $\delta = 3$ on the honeycomb and $\delta = 4$ on the square lattices. The functions $f_k(x)$ and $g_k(x)$ are defined by

$$f_1(x) = \frac{2\sinh[\beta(x+h)]}{2\cosh[\beta(x+h)] + \exp(-\beta D)}, \tag{4}$$

$$f_2(x) = \frac{2\cosh[\beta(x+h)]}{2\cosh[\beta(x+h)] + \exp(-\beta D)}, \tag{5}$$

$$g_1(x) = \frac{\left\{\begin{array}{l} 5\sinh\left[\frac{5\beta}{2}(x+h)\right] + 3\sinh\left[\frac{3\beta}{2}(x+h)\right] \\ \times\exp(-4\beta\Delta) + \sinh\left[\frac{\beta}{2}(x+h)\right]\exp(-6\beta\Delta)\end{array}\right\}}{\left\{\begin{array}{l} 2\cosh\left[\frac{5\beta}{2}(x+h)\right] + 2\cosh\left[\frac{3\beta}{2}(x+h)\right] \\ \times\exp(-4\beta\Delta) + 2\cosh\left[\frac{\beta}{2}(x+h)\right]\exp(-6\beta\Delta)\end{array}\right\}}, \tag{6}$$

$$g_2(x)=\frac{\left\{\begin{array}{l}25\cosh\left[\frac{5\beta}{2}(x+h)\right]+9\cosh\left[\frac{3\beta}{2}(x+h)\right]\\ \times\exp(-4\beta\Delta)+\cosh\left[\frac{\beta}{2}(x+h)\right]\exp(-6\beta\Delta)\end{array}\right\}}{\left\{\begin{array}{l}4\cosh\left[\frac{5\beta}{2}(x+h)\right]+4\cosh\left[\frac{3\beta}{2}(x+h)\right]\\ \times\exp(-4\beta\Delta)+4\cosh\left[\frac{\beta}{2}(x+h)\right]\exp(-6\beta\Delta)\end{array}\right\}}, \tag{7}$$

$$g_3(x)=\frac{\left\{\begin{array}{l}125\sinh\left[\frac{5\beta}{2}(x+h)\right]+27\cosh\left[\frac{3\beta}{2}(x+h)\right]\\ \times\exp(-4\beta\Delta)+\cosh\left[\frac{\beta}{2}(x+h)\right]\exp(-6\beta\Delta)\end{array}\right\}}{\left\{\begin{array}{l}8\cosh\left[\frac{5\beta}{2}(x+h)\right]+8\cosh\left[\frac{3\beta}{2}(x+h)\right]\\ \times\exp(-4\beta\Delta)+8\cosh\left[\frac{\beta}{2}(x+h)\right]\exp(-6\beta\Delta)\end{array}\right\}}, \tag{8}$$

$$g_4(x)=\frac{\left\{\begin{array}{l}625\cosh\left[\frac{5\beta}{2}(x+h)\right]+81\cosh\left[\frac{3\beta}{2}(x+h)\right]\\ \times\exp(-4\beta\Delta)+\cosh\left[\frac{\beta}{2}(x+h)\right]\exp(-6\beta\Delta)\end{array}\right\}}{\left\{\begin{array}{l}16\cosh\left[\frac{5\beta}{2}(x+h)\right]+16\cosh\left[\frac{3\beta}{2}(x+h)\right]\\ \times\exp(-4\beta\Delta)+16\cosh\left[\frac{\beta}{2}(x+h)\right]\exp(-6\beta\Delta)\end{array}\right\}}, \tag{9}$$

$$g_5(x)=\frac{\left\{\begin{array}{l}3125\sinh\left[\frac{5\beta}{2}(x+h)\right]+243\cosh\left[\frac{3\beta}{2}(x+h)\right]\\ \times\exp(-4\beta\Delta)+\cosh\left[\frac{\beta}{2}(x+h)\right]\exp(-6\beta\Delta)\end{array}\right\}}{\left\{\begin{array}{l}32\cosh\left[\frac{5\beta}{2}(x+h)\right]+32\cosh\left[\frac{3\beta}{2}(x+h)\right]\\ \times\exp(-4\beta\Delta)+32\cosh\left[\frac{\beta}{2}(x+h)\right]\exp(-6\beta\Delta)\end{array}\right\}}, \tag{10}$$

where $\beta=1/k_{\mathrm{B}}T$, k_{B} is the Boltzmann constant and T is the absolute temperature. The coefficients $A(a)$, $B(a)$, $C(a)$, $D(a)$, $E(a)$ and $F(a)$ in equation (2) are obtained by using the exact van der Waerden identity

$$\begin{aligned}
A(a)&=\frac{1}{128}\left[3\cosh\left(\frac{5a}{2}\right)-25\cosh\left(\frac{3a}{2}\right)+150\cosh\left(\frac{a}{2}\right)\right],\\
B(a)&=\frac{1}{960}\left[9\sinh\left(\frac{5a}{2}\right)-125\sinh\left(\frac{3a}{2}\right)+2250\sinh\left(\frac{a}{2}\right)\right],\\
C(a)&=\frac{1}{48}\left[-5\cosh\left(\frac{5a}{2}\right)+39\cosh\left(\frac{3a}{2}\right)-34\cosh\left(\frac{a}{2}\right)\right],\\
D(a)&=\frac{1}{24}\left[-\sinh\left(\frac{5a}{2}\right)+13\sinh\left(\frac{3a}{2}\right)-34\sinh\left(\frac{a}{2}\right)\right],\\
E(a)&=\frac{1}{24}\left[\cosh\left(\frac{5a}{2}\right)-3\cosh\left(\frac{3a}{2}\right)+2\cosh\left(\frac{a}{2}\right)\right],\\
F(a)&=\frac{1}{60}\left[\sinh\left(\frac{5a}{2}\right)-5\sinh\left(\frac{3a}{2}\right)+10\sinh\left(\frac{a}{2}\right)\right].
\end{aligned} \tag{11}$$

Equations (2) and (3) are also exact and are valid for any lattice. If we try to exactly treat all the spin–spin correlations for that set of equations, the problem quickly becomes intractable. A first obvious attempt to deal with it is to ignore correlations; the decoupling approximation:

$$\begin{aligned}
\left\langle\sigma_i(\sigma_{i'})^2\ldots\sigma_{i^n}\right\rangle&\cong\langle\sigma_i\rangle\left\langle(\sigma_{i'})^2\right\rangle\cdots\langle\sigma_{i^n}\rangle,\\
\left\langle S_j(S_{j'})^2\ldots(S_{j^n})^5\right\rangle&\cong\langle S_j\rangle\left\langle(S_{j'})^2\right\rangle\cdots\langle(S_{j^n})^5\rangle,
\end{aligned} \tag{12}$$

with $i\neq i'\neq\cdots\neq i^n$ and $j\neq j'\neq\cdots\neq j^n$ have been introduced within the EFT with correlations [51, 53, 63]. In fact, the approximation corresponds essentially to the Zernike approximation [64] in the bulk problem, and has been successfully applied to a great number of magnetic systems including the surface problems [51, 53, 63, 65]. On the other hand, in the mean-field theory, all the correlations, including the self-correlations, are neglected. Based on these approximations, equations (2) and (3) reduce to

$$\begin{aligned}
m_{\mathrm{A}}=&\left[A(a)+B(a)\langle S_j\rangle+C(a)\left\langle(S_j)^2\right\rangle+D(a)\left\langle(S_j)^3\right\rangle\right.\\
&\left.+E(a)\left\langle(S_j)^4\right\rangle+F(a)\left\langle(S_j)^5\right\rangle\right]^{\delta}f_1(x)|_{x=0},
\end{aligned} \tag{13}$$

$$\begin{aligned}
q_{\mathrm{A}}=&\left[A(a)+B(a)\langle S_j\rangle+C(a)\left\langle(S_j)^2\right\rangle+D(a)\left\langle(S_j)^3\right\rangle\right.\\
&\left.+E(a)\left\langle(S_j)^4\right\rangle+F(a)\left\langle(S_j)^5\right\rangle\right]^{\delta}f_2(x)|_{x=0},
\end{aligned} \tag{14}$$

$$\begin{aligned}
m_{\mathrm{B}}=&\left[1+\langle\sigma_i\rangle\sinh(J\nabla)\right.\\
&\left.+\left\langle(\sigma_i)^2\right\rangle\{\cosh(J\nabla)-1\}\right]^{\delta}g_1(x)|_{x=0},
\end{aligned} \tag{15}$$

$$\begin{aligned}
q_{\mathrm{B}}=&\left[1+\langle\sigma_i\rangle\sinh(J\nabla)\right.\\
&\left.+\left\langle(\sigma_i)^2\right\rangle\{\cosh(J\nabla)-1\}\right]^{\delta}g_2(x)|_{x=0},
\end{aligned} \tag{16}$$

$$\begin{aligned}
r_{\mathrm{B}}=&\left[1+\langle\sigma_i\rangle\sinh(J\nabla)\right.\\
&\left.+\left\langle(\sigma_i)^2\right\rangle\{\cosh(J\nabla)-1\}\right]^{\delta}g_3(x)|_{x=0},
\end{aligned} \tag{17}$$

$$\begin{aligned}
\upsilon_{\mathrm{B}}=&\left[1+\langle\sigma_i\rangle\sinh(J\nabla)\right.\\
&\left.+\left\langle(\sigma_i)^2\right\rangle\{\cosh(J\nabla)-1\}\right]^{\delta}g_4(x)|_{x=0},
\end{aligned} \tag{18}$$

$$\begin{aligned}
w_{\mathrm{B}}=&\left[1+\langle\sigma_i\rangle\sinh(J\nabla)\right.\\
&\left.+\left\langle(\sigma_i)^2\right\rangle\{\cosh(J\nabla)-1\}\right]^{\delta}g_5(x)|_{x=0},
\end{aligned} \tag{19}$$

So far we have discussed the basic formulation of the mixed spin-1 and spin-5/2 Ising model with a crystal-field in a longitudinal magnetic field with a coordination number δ; hence equations (13)–(19) can be used to investigate the thermal variations of the sublattice magnetizations and then phase diagrams can be calculated. As one can see, in our treatment new order parameters q_{A}, q_{B}, r_{B}, υ_{B} and w_{B} naturally appear, which one is able to evaluate. This is not the case with the standard MFA where all correlations are neglected. This is one of the reasons why the present framework provides better results than the standard MFA.

2.1. Application to the honeycomb lattice ($\delta=3$)

We are now interested in studying the transition temperature (or the phase diagrams) of the system. Certain features of

the phase diagram can be determined analytically through a Landau free energy expansion in the order parameters. For simplicity, we will discuss in detail the honeycomb lattice with $\delta = 3$ seen in figure 1(a). Putting $\delta = 3$ into equations (13)–(19), and expanding the right-hand sides of these equations, one can obtain the following set of coupled equations:

$$\begin{aligned} m_{\mathrm{A}} = {} & A_0 + A_1 m_{\mathrm{B}} + A_2 m_{\mathrm{B}}^2 + A_3 m_{\mathrm{B}}^3 A_4 m_{\mathrm{B}}^4 + A_5 m_{\mathrm{B}}^5 \\ & + A_6 m_{\mathrm{B}}^6 + A_7 m_{\mathrm{B}}^7 + A_8 m_{\mathrm{B}}^8 + A_9 m_{\mathrm{B}}^9 + A_{10} m_{\mathrm{B}}^{10} \\ & + A_{11} m_{\mathrm{B}}^{11} + A_{12} m_{\mathrm{B}}^{12} + A_{13} m_{\mathrm{B}}^{13} + A_{14} m_{\mathrm{B}}^{14} + A_{15} m_{\mathrm{B}}^{15}, \end{aligned} \tag{20}$$

$$m_{\mathrm{B}} = B_0 + B_1 m_{\mathrm{A}} + B_2 m_{\mathrm{A}}^2 + B_3 m_{\mathrm{A}}^3 + B_4 m_{\mathrm{A}}^4 + B_5 m_{\mathrm{A}}^5 + B_6 m_{\mathrm{A}}^6, \tag{21}$$

where the coefficients A_i $(i = 0, 1, \ldots, 15)$ and B_j $(j = 0, 1, 2, \ldots, 6)$ can be easily calculated by applying mathematical relations $\exp(\alpha\nabla) f(x) = f(x+\alpha)$ and $\exp(\alpha\nabla) g(x) = g(x+\alpha)$ as given in the appendix A. The definitions of the sublattice magnetizations for the honeycomb lattice are $m_{\mathrm{A}} = \langle \sigma_i \rangle$ and $m_{\mathrm{B}} = \langle S_j \rangle$. Solving the coupled equations (20) and (21), we can obtain the magnetization curves for the honeycomb lattice. We will perform this calculation in the next section.

2.2. Application to the square lattice ($\delta = 4$)

In this subsection, we shall obtain the set of coupled equations on the square lattice with $\delta = 4$. For constructing these coupled equations, we need to consider not three- but four-site blocks as seen in figure 1(b). To obtain the set of coupled equations, one can put $\delta = 4$ into equations (13)–(19) and expand the right-hand sides of these equations. The application of equations (13)–(19) to square lattice with $\delta = 4$ leads then to the following set of mutually coupled equations

$$\begin{aligned} m_{\mathrm{A}} = {} & C_0 + C_1 m_{\mathrm{B}} + C_2 m_{\mathrm{B}}^2 + C_3 m_{\mathrm{B}}^3 + C_4 m_{\mathrm{B}}^4 + C_5 m_{\mathrm{B}}^5 \\ & + C_6 m_{\mathrm{B}}^6 + C_7 m_{\mathrm{B}}^7 + C_8 m_{\mathrm{B}}^8 + C_9 m_{\mathrm{B}}^9 + C_{10} m_{\mathrm{B}}^{10} \\ & + C_{11} m_{\mathrm{B}}^{11} + C_{12} m_{\mathrm{B}}^{12} + C_{13} m_{\mathrm{B}}^{13} + C_{14} m_{\mathrm{B}}^{14} + C_{15} m_{\mathrm{B}}^{15} \\ & + C_{16} m_{\mathrm{B}}^{16} + C_{17} m_{\mathrm{B}}^{17} + C_{18} m_{\mathrm{B}}^{18} + C_{19} m_{\mathrm{B}}^{19} + C_{20} m_{\mathrm{B}}^{20}, \end{aligned} \tag{22}$$

$$\begin{aligned} m_{\mathrm{B}} = {} & D_0 + D_1 m_{\mathrm{A}} + D_2 m_{\mathrm{A}}^2 + D_3 m_{\mathrm{A}}^3 + D_4 m_{\mathrm{A}}^4 \\ & + D_5 m_{\mathrm{A}}^5 + D_6 m_{\mathrm{A}}^6 + D_7 m_{\mathrm{A}}^7 + D_8 m_{\mathrm{A}}^8, \end{aligned} \tag{23}$$

where the coefficients C_k $(k = 0, 1, \ldots, 20)$ and D_l $(l = 0, 1, \ldots, 8)$ can be easily calculated by applying mathematical relations $\exp(\alpha\nabla) f(x) = f(x+\alpha)$ and $\exp(\alpha\nabla) g(x) = g(x+\alpha)$ as given in appendix B. The definitions of the sublattice magnetizations for the square lattice are $m_{\mathrm{A}} = \langle \sigma_i \rangle$ and $m_{\mathrm{B}} = \langle S_j \rangle$. Solving the coupled equations (22) and (23), we can obtain the magnetization curves for the square lattice.

2.3. Thermodynamical properties

Now, we illustrate how to calculate the thermodynamical quantities (the susceptibility χ_α, internal energy U and specific heat C) for the system with a crystal-field in a longitudinal magnetic field. The susceptibility for the system can be determined easily from the following equation:

$$\chi_\alpha = \lim_{h \to 0} \frac{\partial m_\alpha}{\partial h}, \tag{24}$$

where α $(\alpha = \mathrm{A}, \mathrm{B})$ are the values of the sublattice magnetizations. Hence, the total longitudinal susceptibility [66] is given by

$$\chi_{\mathrm{T}} = \chi_{\mathrm{A}} + \chi_{\mathrm{B}} = \left.\frac{\partial m_{\mathrm{A}}}{\partial h}\right|_{h=0} + \left.\frac{\partial m_{\mathrm{B}}}{\partial h}\right|_{h=0}. \tag{25}$$

The internal energy per site of the system can be obtained from the thermodynamic average of the Hamiltonian. In the traditional method [67], the internal energy U of the mixed-spin system is given by

$$\begin{aligned} \frac{U}{N} = {} & -\frac{1}{2}\langle \sigma_i E_i \rangle - \frac{1}{2}\langle S_j E_j \rangle - \Delta \left(\left\langle (\sigma_i)^2 \right\rangle \right. \\ & \left. + \left\langle (S_j)^2 \right\rangle \right) - h \left(\langle \sigma_i \rangle + \langle S_j \rangle \right), \end{aligned} \tag{26}$$

with $E_i = -J \sum_\delta S_{j+\delta}$ and $E_j = -J \sum_\delta \sigma_{i+\delta}$, where the summations are over the nearest neighbors of a site i (or a site j). $\langle \sigma_i E_i \rangle$ and $\langle S_j E_j \rangle$ can be written as

$$\begin{aligned} \langle \sigma_i E_i \rangle = {} & zJ \left[A(a) + B(a)\langle S_j \rangle + C(a) \left\langle (S_j)^2 \right\rangle \right. \\ & \left. + D(a) \left\langle (S_j)^3 \right\rangle + E(a) \left\langle (S_j)^4 \right\rangle + F(a) \left\langle (S_j)^5 \right\rangle \right]^{\delta - 1} \\ & \times \frac{\partial}{\partial \nabla} \left[A(a) + B(a)\langle S_j \rangle + C(a) \left\langle (S_j)^2 \right\rangle \right. \\ & \left. + D(a) \left\langle (S_j)^3 \right\rangle + E(a) \left\langle (S_j)^4 \right\rangle + F(a) \left\langle (S_j)^5 \right\rangle \right] \\ & \times f_1(x)|_{x=0}, \end{aligned} \tag{27}$$

$$\begin{aligned} \langle S_j E_j \rangle = {} & zJ \left[1 + \langle \sigma_i \rangle \sinh(J\nabla) + \left\langle (\sigma_i)^2 \right\rangle (\cosh(J\nabla) - 1) \right]^{\delta - 1} \\ & \times \frac{\partial}{\partial \nabla} \left[1 + \langle \sigma_i \rangle \sinh(J\nabla) + \left\langle (\sigma_i)^2 \right\rangle (\cosh(J\nabla) - 1) \right] g_1(x)|_{x=0}. \end{aligned} \tag{28}$$

It is clear that for the evaluation of internal energy U, we must know equations (26)–(28), and also the parameters m_{A}, m_{B}, q_{A}, q_{B}, r_{B}, v_{B} and w_{B}. Then, these quantities can be easily obtained by solving equations (13)–(19) numerically.

Finally, the specific heat C of the system can be determined from the relation

$$C = \frac{\partial U}{\partial T}. \tag{29}$$

3. Numerical results and discussions

In this section, we examine some interesting and typical results for the mixed spin-1 and spin-5/2 Ising model with a crystal-field in a longitudinal magnetic field. Numerical results and discussions are given only for a honeycomb lattice for the reason that these results are similar for a square lattice, except that the critical temperature occurs at high values.

Table 1. All possible spin configurations of the model, their respective energies and the conditions for the existence of the configurations.

Two-site blocks	Energy	Condition
$\langle -1-5/2\rangle$	$-\frac{5}{2}J+\frac{7}{2}h-\frac{29}{4}\Delta$	$5J-2h>0$, $J-h+4\Delta<0$ and $5J-2h+2\Delta>0$
$\langle -1-3/2\rangle$	$-\frac{3}{2}J+\frac{5}{2}h-\frac{13}{4}\Delta$	$J-2\Delta>0$, $J-h+2\Delta>0$ and $J-h+4\Delta<0$
$\langle -1-1/2\rangle$	$-\frac{J}{2}+\frac{3}{2}h-\frac{5}{4}\Delta$	$J-2\Delta>0$, $J-2h+2\Delta>0$ and $J-h+2\Delta<0$
$\langle -1+3/2\rangle$	$\frac{3}{2}J-\frac{1}{2}h-\frac{13}{4}\Delta$	$h>0$, $J-2\Delta<0$ and $J-h-4\Delta>0$
$\langle -1+5/2\rangle$	$\frac{5}{2}J-\frac{3}{2}h-\frac{29}{4}\Delta$	$h>0$, $J-2\Delta<0$, $J-h-4\Delta<05J+2h<0$ and $5J+2h-2\Delta<0$
$\langle +1-5/2\rangle$	$\frac{5}{2}J+\frac{3}{2}h-\frac{29}{4}\Delta$	$h<0$, $J-2\Delta<0$, $J+h-4\Delta<05J-2h<0$ and $5J-2h-2\Delta<0$
$\langle +1-3/2\rangle$	$\frac{3}{2}J+\frac{1}{2}h-\frac{13}{4}\Delta$	$h<0$, $J+h-4\Delta>0$ and $J-2\Delta<0$
$\langle +1+1/2\rangle$	$-\frac{J}{2}-\frac{3}{2}h-\frac{5}{4}\Delta$	$J-2\Delta>0$, $J+2h+2\Delta<0$ and $J+h+2\Delta<0$
$\langle +1+3/2\rangle$	$-\frac{3}{2}J-\frac{5}{2}h-\frac{13}{4}\Delta$	$J+h+4\Delta<0$, $J+h+2\Delta>0$ and $J-2\Delta>0$
$\langle +1+5/2\rangle$	$-\frac{5}{2}J-\frac{7}{2}h-\frac{29}{4}\Delta$	$J+h+4\Delta>0$, $5J+2h+2\Delta>0$ and $5J+2h>0$
$\langle 0+5/2\rangle$	$-\frac{5}{2}h-\frac{25}{4}\Delta$	$J-2\Delta<0$, $5J+2h-2\Delta>0$ and $5J+2h+2\Delta<0$
$\langle 0+1/2\rangle$	$-\frac{h}{2}-\frac{\Delta}{4}$	$J+2h+2\Delta<0$, $J-2\Delta>0$ and $h>0$
$\langle 0-1/2\rangle$	$\frac{h}{2}-\frac{\Delta}{4}$	$J-2h+2\Delta<0$, $J-2\Delta>0$ and $h<0$
$\langle 0-5/2\rangle$	$\frac{5}{2}h-\frac{25}{4}\Delta$	$J-2\Delta<0$, $5J-2h-2\Delta>0$ and $5J-2h+2\Delta<0$

3.1. Ground-state phase diagram

Since the ground-state phase diagram can be exactly obtained and it can be used to check the reliability of the theoretical results, we start our investigation by calculating the ground-state phase diagram. The ground state phase diagram is obtained in the $h/\delta|J|$ versus $\Delta/\delta|J|$ plane from the condition of the minimum energy value of the configuration by comparing with the energy of the other configurations for a given set of the parameters, as seen in figure 2. Each one of these configurations for the given system parameters correspond to the stable states of the model. Hence, we have found 14 possible spin configurations; the respective energies and the condition for their existence are given in table 1. All possible spin configurations are also indicated in the ground-state phase diagram, as seen in figure 2. It has ten multicritical points where more than one phase can coexist, namely $a_1, a_2, \ldots, a_{10}$. The multiphase lines separate the phases; for example, the multiphase line a_4–a_5 separates the ferrimagnetic $(-1, 5/2)$ phase from the ferrimagnetic $(-1, 3/2)$ phase.

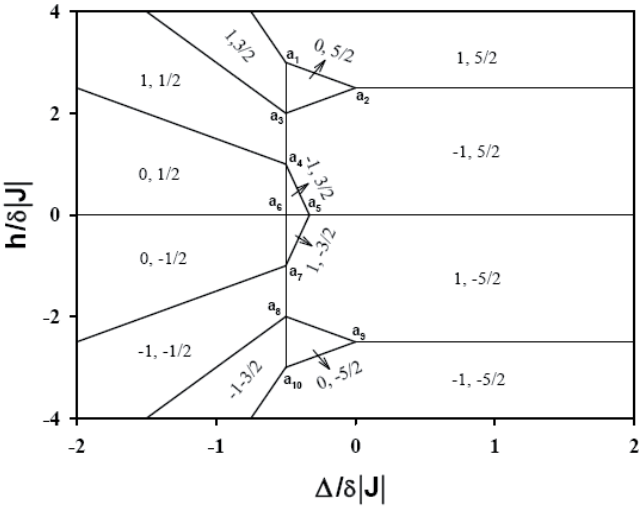

Figure 2. The ground-state phase diagram of the mixed spin-1 and spin-5/2 Ising model in the $(h/\delta|J|, \Delta/\delta|J|)$ plane for $J<0$. The spin configurations, the respective energies and the conditions for the existence of the phases are represented by the labels given in table 1.

3.2. Phase diagrams

In this subsection, we shall show some typical results for the mixed spin-1 and spin-5/2 Ising model with a crystal-field at zero longitudinal magnetic field. We have obtained the phase diagrams by solving equations (20) and (21), and equations (22) and (23) for honeycomb and square lattices, respectively. First, we present the phase diagrams of the model in the $(\Delta/|J|, k_B T/|J|)$ plane for the honeycomb ($\delta=3$) and square ($\delta=4$) lattices, illustrated in figure 3. In these phase diagrams, the solid and dashed lines represent the second- and first-order phase transition lines for both honeycomb and square lattices, respectively, and the tricritical points are denoted by filled circles. It is clear that the second- and first-order phase transition lines separate the ferrimagnetic phases from the paramagnetic (P) phase. The gray and black triangles are the separating points for the honeycomb and square lattices, respectively, and they correspond to the a_5 multicritical points that are marked in the ground-state phase diagram, as seen in figure 2. These triangles separate the ferrimagnetic $(-1, 3/2)$ phase from the ferrimagnetic $(-1, 5/2)$ phase. The following interesting phenomena are observed from the phase diagram: (i) The system exhibits a tricritical point where the second-order phase transition turns to a first-order one. (ii) When the $\Delta/|J|$ values are bigger than the separating point value, the second-order phase transition occurs from the ferrimagnetic $(-1, 5/2)$ phase to the P phase. (iii) When the $\Delta/|J|$ values are between the separating and tricritical points, again the systems on honeycomb and square lattices undergo second-order phase transition; the transition is from the ferrimagnetic $(-1, 3/2)$ phase to the P phase. (iv) Below the tricritical

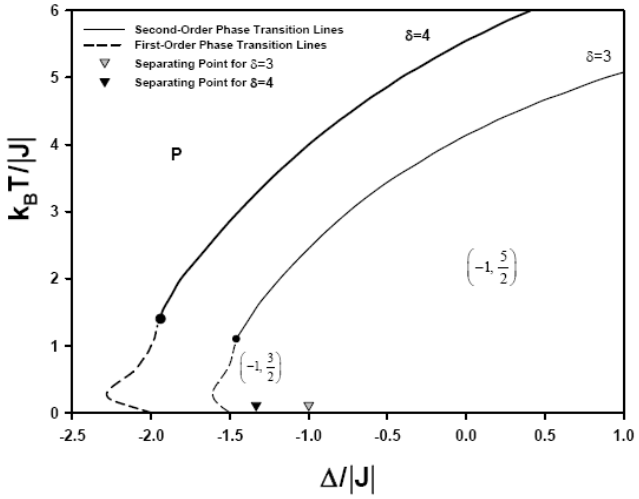

Figure 3. Phase diagrams in the $(\Delta/|J|, k_BT/|J|)$ plane for the mixed spin Ising model consisting of spins $\sigma = 1$ and $S = 5/2$ within the EFT at zero longitudinal magnetic field for both the honeycomb and square lattices. The solid and dashed lines represent the second- and first-order phase transition lines, respectively, for both honeycomb and square lattices; the tricritical points are denoted by filled circles; the gray and black triangles are the separating points for the honeycomb and square lattices, respectively, and they correspond to the a_5 multicritical points that are marked in the ground-state phase diagram. These triangles separate the ferrimagnetic $(-1, 3/2)$ phase from the ferrimagnetic $(-1, 5/2)$ phase.

point, both systems undergo a first-order phase transition in a certain range of $\Delta/|J|$, and the transition is from the ferrimagnetic $(-1, 3/2)$ phase to the P phase. Moreover, both phase diagrams exhibit reentrant behavior for low values of T, i.e. as the temperature increases, the system passes from the P phase to the ferrimagnetic $(-1, 3/2)$ phase, and then back to the P phase again. In spin systems, the reentrant behavior can be understood as follows. At high temperatures, the entropy is the most important factor and uncorrelated fluctuations determine the thermodynamics. The system is then in the P phase bias due to the applied field. As the temperature is lowered, the energy and entropy are both important and the correlated fluctuations affect the dominance of either phase significantly. The system enters the ordered phase. At low temperatures, the energy is important, not the entropy and the system reenters the P phase again [68]. We have found similar phase diagrams to the one seen in the phase diagrams of the MC study of the two-dimensional quadratic mixed spin (1/2, 1) Ising model with crystal-field interaction [2], the mixed spin (1/2, 1) Ising ferrimagnetic system on the Bethe lattice [19], the EFT study of the mixed (1, 3/2) Ising ferrimagnetic system [14], the MFA of the mixed spin (1, 3/2) Ising system [12], the mixed spin (1, 3/2) Ising model on the Bethe lattice [36] and MC studies of critical phenomena in the mixed spin (1, 3/2) BC Ising model on a simple cubic lattice [15].

3.3. Magnetization curves and susceptibilities

Thermal behavior of the sublattice magnetizations (m_A and m_B) and corresponding susceptibilities χ_α ($\alpha = A, B$, total) are illustrated in figure 4. We have obtained thermal behavior

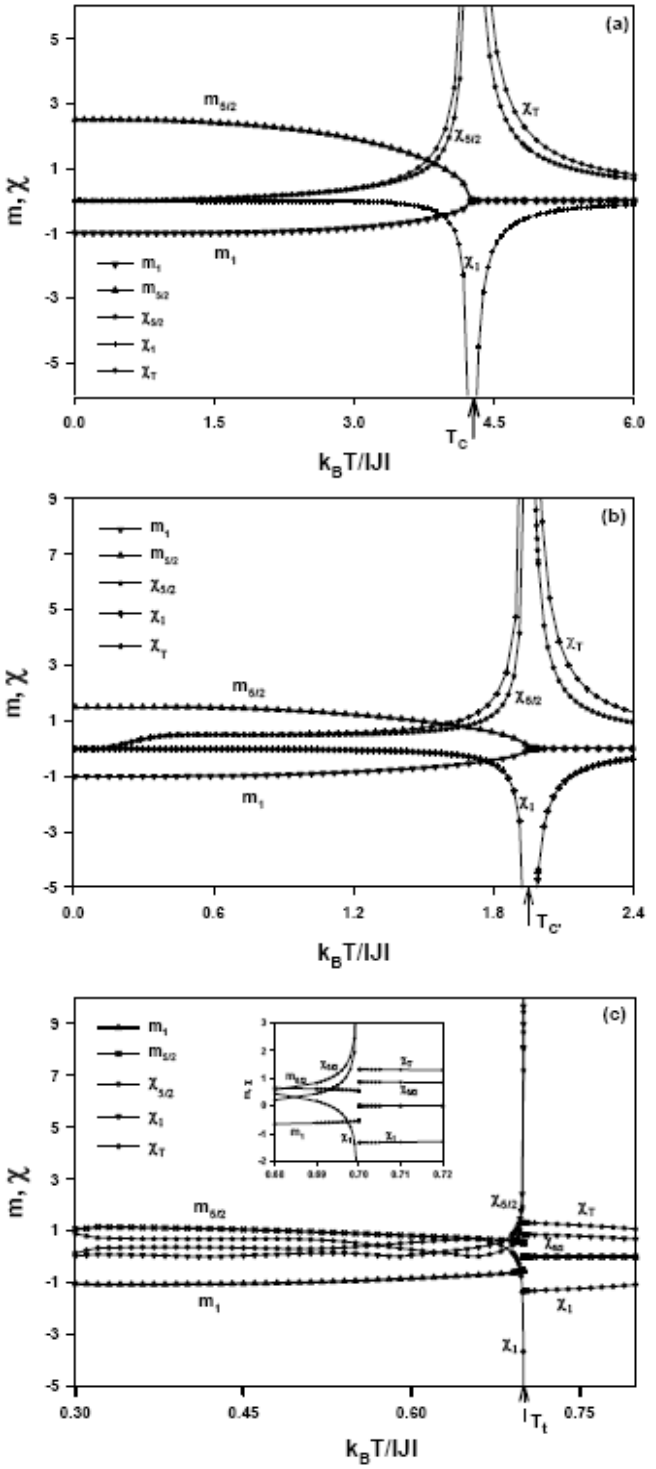

Figure 4. The behavior of the sublattice magnetizations and magnetic susceptibilities as a function of temperature on the honeycomb lattice ($h = 0$). T_C (thick arrow) and $T_{C'}$ (thin arrow) are the second-order phase transition temperatures from the ferrimagnetic $(-1, 5/2)$ phase to the paramagnetic (P) phase; and from the ferrimagnetic (1, 3/2) phase to the P phase, respectively. T_t (dashed arrow) represents the first-order phase transition temperature from the ferrimagnetic (1, 3/2) phase to the P phase. (a) Exhibiting a second-order phase transition from the ferrimagnetic $(-1, 5/2)$ phase to the P phase for $\Delta/|J| = 0.1$; 4.248 is found for T_C. (b) Exhibiting a second-order phase transition from the ferrimagnetic $(-1, 3/2)$ phase to the P phase for $\Delta/|J| = -1.2$; 1.95 is found for $T_{C'}$. (c) Exhibiting a first-order phase transition from the ferrimagnetic $(-1, 3/2)$ phase to the P phase for $\Delta/|J| = -1.5$; 0.699 is found for T_t.

of sublatice magnetizations and corresponding susceptibilities by solving equations (20) and (21), and equations (20), (21) and (25), respectively. We present a few representative graphs to display their behavior for only a honeycomb lattice, seen in figures 4(a)–(c). The results are depicted in figures 4(a)–(c) for the system with zero longitudinal magnetic field ($h = 0$), when the values of $\Delta/|J|$ are 0.1, -1.2 and -1.5, respectively. In these figures, T_C (thick arrow) and $T_{C'}$ (thin arrow) are the second-order phase transition temperatures from the ferrimagnetic $(-1, 5/2)$ phase to the P phase and from the ferrimagnetic $(-1, 3/2)$ phase to the P phase, respectively. T_t (dashed arrow) represents the first-order phase transition temperature from the ferrimagnetic $(-1, 3/2)$ phase to the P phase. It is seen from figure 4(a) for $\Delta/|J| = 0.1$ that the system undergoes a second-order phase transition from the ferrimagnetic $(-1, 5/2)$ phase to the P phase, because sublattice magnetizations go to zero continuously as the temperature increases and a second-order phase transition occurs at $T_C = 4.248$. When the temperature approaches T_C, the sublattice susceptibility $\chi_{5/2}$ increases very rapidly and goes to positive infinity at $T_C = 4.248$. On the other hand, the other sublattice susceptibility χ_1 decreases very rapidly and goes to negative infinity at $T_C = 4.248$. The total susceptibility χ_T exhibits the usual temperature behavior in the vicinity of T_C, $\chi_T \to +\infty$ as $T \to T_C$. This has also been tested by our sublattice magnetizations and susceptibilities calculations, because we found exactly the same T_C for both calculations. Figure 4(b) illustrates the thermal variations of m_1, $m_{5/2}$ and χ_α for $\Delta/|J| = -1.2$, and the behavior of figure 4(b) is similar to figure 4(a), except that the system undergoes a second-order phase transition from the ferrimagnetic $(-1, 3/2)$ phase to the P phase at $T_{C'} = 1.95$. Figure 4(c) is calculated for $\Delta/|J| = -1.5$ and shows m_1, $m_{5/2}$ go to zero discontinuously as the temperature increases; hence a first-order phase transition occurs at $T_t = 0.699$. Moreover, in the vicinity of T_t the sublattice susceptibility $\chi_{5/2}$ rapidly increases for $T < T_t$ and suddenly decreases for $T > T_t$. On the other hand, χ_1 decreases very rapidly for $T < T_t$ and suddenly increases for $T > T_t$. If one compares the behavior of sublattice magnetizations and susceptibilities, one can see that T_t is found to be exactly the same for both calculations.

3.4. Internal energy and specific heat

In order to study the present system in detail, temperature variations of the internal energy and specific heat per site have also been investigated. Let us study the thermal variation of the internal energy and specific heat of the system for the honeycomb lattice by solving equations (20), (21), (26) and (29) numerically. In the case of $h = 0$, we have plotted the temperature dependence of the internal energy and specific heat with $\delta = 3$ for selected values of $\Delta/|J|$, i.e. 1.0, 0.5, 0.0, -0.5, -1.0, -1.47 and -1.5 in figure 5. Figure 5(a) shows that when $T < T_C$ or $T > T_C$ the specific heat for the second-order phase transition increases with increasing temperature. The specific heats may express the discontinuity at $T = T_C$, although in the high-temperature region ($T > T_C$) they take finite values. As to the specific heat, its behavior is very similar to that of the mixed spin-1/2 and spin-3/2 ferro- and ferrimagnetic system [61], the mixed spin-3/2 and spin-5/2 ferrimagnetic system [44] and the mixed spin-1/2 and spin-5/2 ferrimagnetic system [41]. Figure 5(b) illustrates the behavior of the internal energy. It expresses a discontinuity of the curvature at the critical temperature T_C. In the figures, the maxima of the specific heat C correspond to the points where the first-order derivatives of the internal energy U are discontinuous, at which the second-order phase transitions occur. This behavior is consistent with previous studies on mixed spin-1 and spin-2 [47] and mixed spin-2 and spin-5/2 [48, 49]. Figure 5(c) shows the temperature dependences of the specific heat, when the phase transition is first order and $\Delta/|J| = -1.47$ and $\Delta/|J| = -1.5$. At the first-order phase transition temperature, the specific heat C arrives at a maximum value, and then reduces suddenly to a small value. The corresponding internal energies are given in figure 5(d). In this figure, the internal energies increase with increasing temperature discontinuously at the first-order phase transition temperature.

3.5. Effects of the longitudinal magnetic field on the magnetic quantities

We shall investigate the influence of the longitudinal magnetic field on the sublattice magnetizations, susceptibility, specific heat and internal energy for the honeycomb lattice. In figures 6(a)–(d) the temperature dependences of sublattice magnetizations, susceptibility, specific heat and internal energy, respectively, are depicted for different values of $h/\delta|J| = 0.0$, 0.75, 1.50, 2.25, 3.0 and $\Delta/|J| = 0.1$. The numbers on the curves are the values of the longitudinal magnetic field. In figure 6(a), sublattice magnetizations $m_A = 5/2$ and $m_B = -1$ at zero temperature; they decrease to zero continuously as the temperature increases; therefore a second-order phase transition occurs at $T_C = 4.248$ in the case of $h/\delta|J| = 0$. In the presence of a longitudinal magnetic field, the behavior of the magnetic quantities is different from the absence of $h/\delta|J|$. It can be clearly seen that the sublattice magnetizations decrease slowly from their saturation magnetizations to small constant magnetizations with increasing temperature. Moreover, the remaining magnetizations become larger as the applied magnetic field increases. In figure 6(b), we have given the numerical results of the susceptibility of the system in the $(\chi, k_B T/J)$ plane for several values of $h/\delta|J|$. Our results are in good agreement with those of previous works [69–71]. As seen from this figure, in the absence of longitudinal magnetic field, the curves of susceptibility rapidly increase and exhibit a peak at the second-order phase transition temperature and then rapidly decrease as the temperature increases. In the presence of a longitudinal magnetic field, the critical temperature is removed, and the higher the longitudinal magnetic field, the smaller is the susceptibility, reflecting the fact that the longitudinal magnetization is weaker. Finally, the specific heat and internal energy of the system as a function of temperature are depicted in figures 6(c) and (d), respectively, at the selected values of $h/\delta|J| = 0.0$, 0.75, 1.50, 2.25 and 3.0. The specific heat of the system exhibits a second-order phase transition at the transition temperature $T_C = 4.248$ in the case of $h/\delta|J| = 0$, and rapidly decreases

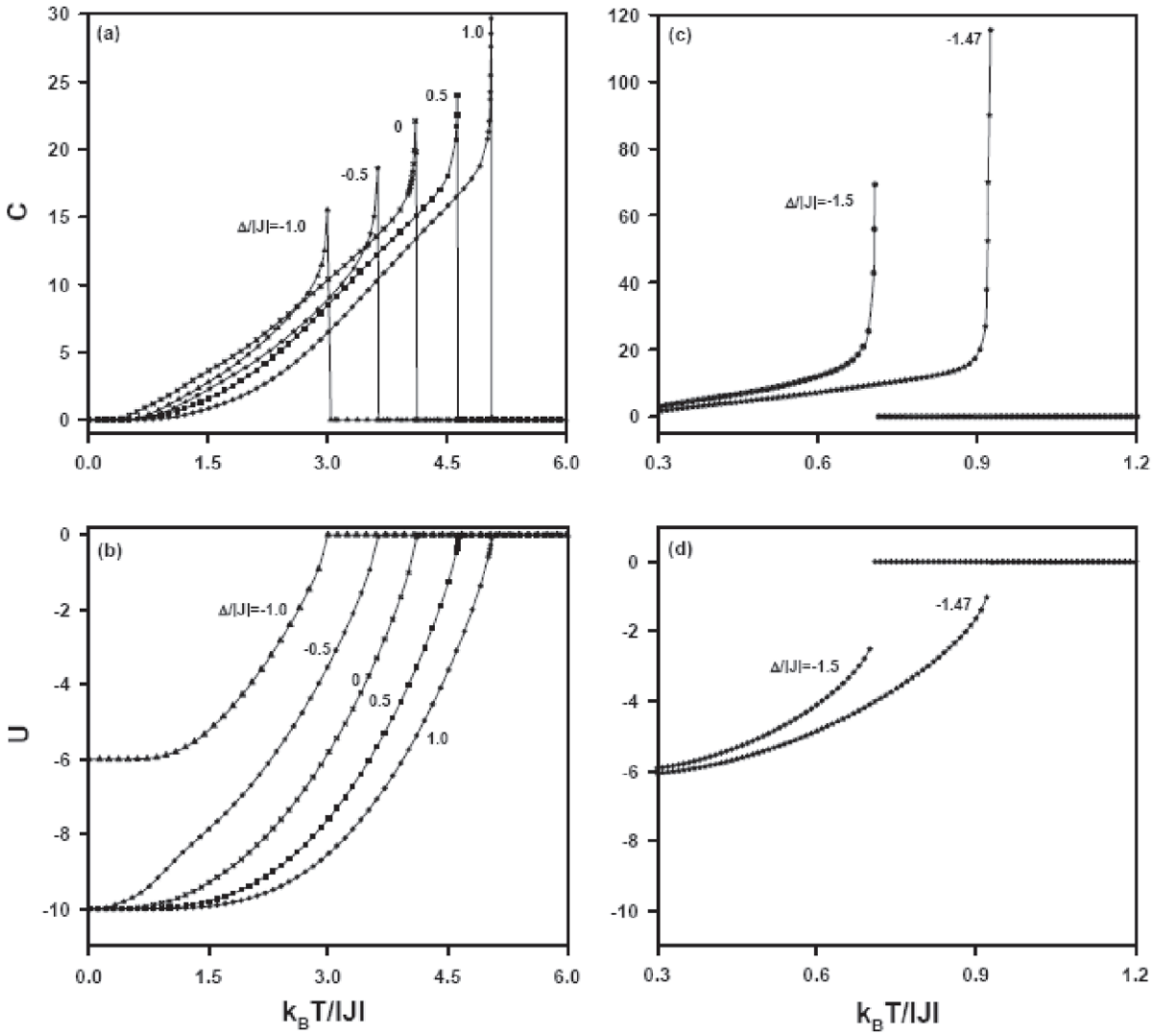

Figure 5. Temperature dependence of the specific heat C and internal energy U for the model on the honeycomb lattice ($h = 0$). (a) Specific heats at the selected values of $\Delta/|J|$, i.e. 1.0, 0.5, 0.0, -0.5 and -1.0. (b) Internal energies at the selected values of $\Delta/|J|$, i.e. 1.0, 0.5, 0.0, -0.5 and -1.0. (c) Specific heats at the selected values of $\Delta/|J|$, i.e. -1.47 and -1.5. (d) Internal energies at the selected values of $\Delta/|J|$, i.e. -1.47 and -1.50.

with increasing temperature. In the presence of $h/\delta|J|$, the critical temperature has been removed. As is seen in figure 6(c), an interesting phenomenon is observed in the low-temperature region $T < T_C$ of the specific heat. The curves show two maxima. Here, the anomalous behavior of specific heat comes from the following fact: for the system with the values of $\Delta/|J| = 0.1$ and $h/\delta|J| = 1.50$ and 2.25 in the vicinity of the critical value ($h/\delta|J| = 2.5$ in the ground-state phase diagram) between the ferrimagnetic $(-1, 5/2)$ phase and the ferrimagnetic $(1, 5/2)$ phase, the ground-state spin configuration may change from $\sigma_i = -1$ to $\sigma_i = +1$. Therefore, the first maximum occurs when $h/\delta|J|$ values approach the critical point and disappears when $h/\delta|J|$ values are far from the critical value. For example, since $h/\delta|J| = 0.75$ and 3.0 are much more different from the critical value ($h/\delta|J| = 2.5$), a first maximum does not exist anymore. One should note that the same feature has been obtained in some similar Ising spin systems [44, 56, 66, 72]. We can also see that the internal energy exhibits a discontinuity in its curvature at the transition temperature $T_C = 4.248$, for $h/\delta|J| = 0$. If the longitudinal magnetic field is different from zero, the critical temperature does not occur in the system. We have found similar behavior to that seen in the previous works [69–71].

4. Summary and conclusions

In this paper, we have studied the magnetic properties of the ferrimagnetic mixed spin-1 and spin-5/2 Ising system with a crystal-field in the absence and presence of longitudinal magnetic field (h) on the honeycomb ($\delta = 3$) and square ($\delta = 4$) lattices by using the EFT with correlations. The ground state phase diagram of the model is obtained in the longitudinal magnetic field (h) and a single-ion potential or crystal-field interaction (Δ) plane, given in figure 2. We also investigated the thermal variations of the sublattice magnetizations and corresponding susceptibilities, seen in figure 4; and present the phase diagrams in the $(\Delta/|J|, k_B T/|J|)$ plane for $h = 0$, shown in figure 3. We have found that the system undergoes the second- and first-order phase transitions; hence the system exhibits a

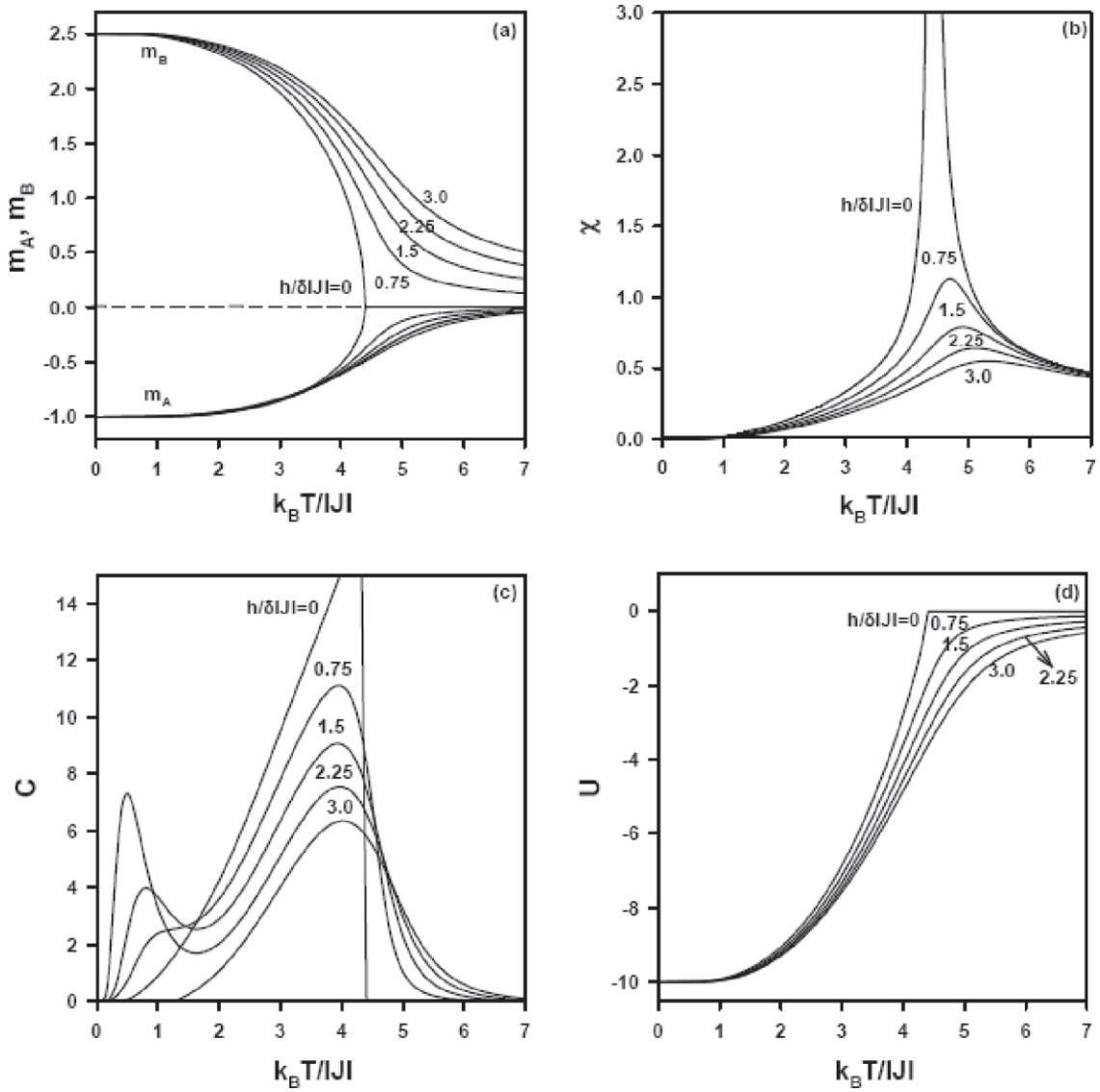

Figure 6. The temperature dependence of the sublattice magnetizations, susceptibility χ, specific heat C and internal energy U for the model on the honeycomb lattice for $\Delta/|J| = 0.1$ at the selected values of $h/\delta|J|$, i.e. 0.0, 0.75, 1.50, 2.25 and 3.0. (a) For sublattice magnetizations m_1, $m_{5/2}$; (b) for susceptibilities χ; (c) for specific heats C and (d) for internal energies U.

tricritical point. The system also displays reentrant behavior for both the honeycomb and square lattice. Other relevant thermodynamical quantities have been evaluated, such as the magnetic susceptibility χ, internal energy U and specific heat C, seen in figures 4 and 5. We have found that χ diverges at the critical temperatures. The maxima of the specific heat C correspond to the points where the first-order derivatives of the internal energy U are discontinuous, at which the second-order phase transitions occur. All the results are in perfect agreement with the ones existing in the literature [44, 47–49, 61, 69–71]. The results are discussed in detail for the present system with and without longitudinal magnetic field.

The influence of longitudinal magnetic field on the sublattice magnetizations, total magnetization, susceptibility, specific heat and internal energy has been discussed in detail, seen in figure 6. The stronger the longitudinal magnetic field, the smaller are the susceptibility and specific heat, reflecting the fact that magnetization is weaker. However, susceptibility, internal energy and specific heat of the system are numerically examined, and some interesting phenomena in these quantities are found due to the applied longitudinal magnetic field. It yields some reasonable results in comparison with those of the other works. Moreover, experimental evidence of the effect of a longitudinal magnetic field can be found in references [73–75].

Acknowledgments

A part of this work was supported by the Scientific and Technological Research Council of Turkey (TÜBİTAK) (grant no. 107T533) and the Erciyes University Research Funds (grant no. FBA-06-01 and FBD-08-593). BD expresses his gratitude to the TÜBİTAK for support through a PhD scholarship.

Appendix A

The coefficients A_i ($i=0, 1, \ldots, 15$) and B_j ($j=0, 1, \ldots, 6$) in equations (20) and (21) can be easily calculated by using

the mathematical relations $\exp(\alpha\nabla)f(x) = f(x+\alpha)$ and $\exp(\alpha\nabla)g(x) = g(x+\alpha)$, where $\nabla = \partial/\partial x$ is a differential operator. These coefficients A_i $(i = 0, 1, \ldots, 15)$ and B_j $(j = 0, 1, 2, \ldots 6)$ are obtained as follows:

$$\begin{aligned}A_0 = \tfrac{1}{16\,777\,216}[&27f_1(-15J/2) - 675f_1(-13J/2)\\ &+9675f_1(-11J/2) - 79\,075f_1(-9J/2)\\ &+415\,575f_1(-7J/2) - 989\,919f_1(-5J/2)\\ &+86\,775f_1(-3J/2) + 8946\,225f_1(-J/2)\\ &+8946\,225f_1(J/2) + 86\,775f_1(3J/2)\\ &-989\,919f_1(5J/2) + 415\,575f_1(7J/2)\\ &-79\,075f_1(9J/2) + 9675f_1(11J/2)\\ &-675f_1(13J/2) + 27f_1(15J/2)],\end{aligned}$$

$$\begin{aligned}A_{15} = \tfrac{1}{1728\,000}[&-f_1(-15J/2) + 15f_1(-13J/2)\\ &-105f_1(-11J/2) + 455f_1(-9J/2) - 1365f_1(-7J/2)\\ &+3003f_1(-5J/2) - 5005f_1(-3J/2) + 6345f_1(-J/2)\\ &-6345f_1(J/2) + 5005f_1(3J/2) - 3003f_1(5J/2)\\ &+1365f_1(7J/2) - 455f_1(9J/2) + 105f_1(11J/2)\\ &-15f_1(13J/2) + f_1(15J/2)],\end{aligned}$$

$$\begin{aligned}B_0 &= g_1(0),\\ B_1 &= \tfrac{3}{2}[-g_1(-J) + g_1(J)],\\ B_2 &= \tfrac{3}{4}[-6g_1(0) + g_1(-2J) + 2g_1(-J) + 2g_1(J) + g_1(2J)],\\ B_3 &= \tfrac{1}{8}[-g_1(-3J) - 12g_1(-2J) + 27g_1(-J) - 27g_1(J)\\ &\quad + 12g_1(2J) + g_1(3J)],\\ B_4 &= \tfrac{3}{8}[16g_1(0) + g_1(-3J) - 9g_1(-J) - 9g_1(J) + g_1(3J)],\\ B_5 &= \tfrac{3}{8}[-g_1(-3J) + 4g_1(-2J) - 5g_1(-J) + 5g_1(J)\\ &\quad - 4g_1(2J) + g_1(3J)],\\ B_6 &= \tfrac{1}{8}[-20g_1(0) + g_1(-3J) - 6g_1(-2J) + 15g_1(-J)\\ &\quad + 15g_1(J) - 6g_1(2J) + g_1(3J)].\end{aligned}$$

Appendix B

The coefficients C_k $(k = 0, 1, \ldots, 20)$ and D_l $(l = 0, 1, \ldots, 8)$ in equations (22) and (23) can be easily calculated by the same way. These coefficients are obtained as follows:

$$\begin{aligned}C_0 = \tfrac{1}{4294\,967\,296}[&81f_1(-10J) - 2700f_1(-9J)\\ &+49\,950f_1(-8J) - 576\,300f_1(-7J) + 4572\,925f_1(-6J)\\ &-23\,752\,176f_1(-5J) + 75\,239\,400f_1(-4J)\\ &-59\,476\,400f_1(-3J) - 342\,915\,150f_1(-2J)\\ &+1157\,549\,400f_1(-J) + 2673\,589\,236f_1(0)\\ &+1157\,549\,400f_1(J) - 342\,915\,150f_1(2J)\\ &-59\,476\,400f_1(3J) + 75\,239\,400f_1(4J)\\ &-23\,752\,176f_1(5J) + 4572\,925f_1(6J) - 576\,300f_1(7J)\\ &+49\,950f_1(8J) - 2700f_1(9J) + 81f_1(10J)],\end{aligned}$$

$$\begin{aligned}C_{20} = \tfrac{1}{207\,360\,000}[&f_1(-10J) - 20f_1(-9J) + 190f_1(-8J)\\ &-1140f_1(-7J) + 4845f_1(-6J) - 15\,504f_1(-5J)\\ &+38\,760f_1(-4J) - 77\,520f_1(-3J) + 125\,970f_1(-2J)\\ &-167\,960f_1(-J) + 184\,756f_1(0) - 167\,960f_1(J)\\ &+125\,970f_1(2J) - 77\,520f_1(3J) + 38\,760f_1(4J)\\ &-15\,504f_1(5J) + 4845f_1(6J) - 1140f_1(7J)\\ &+190f_1(8J) - 20f_1(9J) + f_1(10J)],\end{aligned}$$

$$\begin{aligned}D_0 &= [g_1(0)],\\ D_1 &= 2[-g_1(-J) + g_1(J)],\\ D_2 &= \tfrac{1}{2}[-14g_1(0) + 3g_1(-2J) + 4g_1(-J) + 4g_1(J) + 3g_1(2J)],\\ D_3 &= \tfrac{1}{2}[-g_1(-3J) - 6g_1(-2J) + 15g_1(-J) - 15g_1(J)\\ &\quad + 6g_1(2J) + g_1(3J)],\\ D_4 &= \tfrac{1}{16}[246g_1(0) + g_1(-4J) + 24g_1(-3J)\\ &\quad - 8g_1(-2J) - 120g_1(-J) - 120g_1(J)\\ &\quad - 28g_1(2J) + 24g_1(3J) + g_1(4J)],\\ D_5 &= \tfrac{1}{4}[-g_1(-4J) - 4g_1(-3J) + 26g_1(-2J) - 36g_1(-J)\\ &\quad + 36g_1(J) - 26g_1(2J) + 4g_1(3J) + g_1(4J)],\\ D_6 &= \tfrac{1}{8}[-110g_1(0) + 3g_1(-4J) - 8g_1(-3J) - 12g_1(-2J)\\ &\quad + 72g_1(-J) + 72g_1(J) - 12g_1(2J) - 8g_1(3J) + 3g_14J)],\\ D_7 &= \tfrac{1}{4}[-g_1(-4J) + 6g_1(-3J) - 14g_1(-2J) + 14g_1(-J)\\ &\quad - 14g_1(J) + 14g_1(2J) - 6g_1(3J) + g_1(4J)],\\ D_8 &= \tfrac{1}{16}[70g_1(0) + g_1(-4J) - 8g_1(-3J) + 28g_1(-2J)\\ &\quad - 56g_1(-J) - 56g_1(J) + 28g_1(2J) - 8g_1(3J) + g_1(4J)].\end{aligned}$$

References

[1] Iwashita T and Uryu N 1984 *Phys. Status Solidi* b **125** 551
[2] Zhang G M and Yang Ch Z 1993 *Phys. Rev.* B **48** 9452
[3] Kaneyoshi T 1999 *Physica* A **272** 545
[4] Kasama T, Muraoka Y and Idogaki T 2006 *Phys. Rev.* B **73** 214411
[5] Belmamoun Y and Kerouad M 2008 *Phys. Scr.* **77** 025706
[6] Benayad N, Dakhama A, Klumper A and Zittartz J 1996 *Z. Phys.* B **101** 623
[7] Bobak A and Jurčišin M 1996 *J. Magn. Magn. Mater.* **163** 292
[8] Buendía G M and Cardona R 1999 *Phys. Rev.* B **59** 6784
[9] Albayrak E and Akkaya S 2007 *Phys. Scr.* **76** 354
[10] Essaoudi I, Barner K and Ainane A 2007 *Physica* A **385** 208
[11] Bobák A and Jurčišin M 1997 *Physica* B **233** 187
[12] Abubrig O F, Horvath D, Bobak A and Jaščur M 2001 *Physica* A **296** 437
[13] Tucker J W 2001 *J. Magn. Magn. Mater.* **237** 215
[14] Bobak A, Abubrig O F and Horvath D 2002 *J. Magn. Magn. Mater.* **246** 177
[15] Wei G Z, Zhang Q and Gu Y W 2006 *J. Magn. Magn. Mater.* **301** 245.

[16] Goncalves L L 1985 *Phys. Scr.* **32** 248
Goncalves L L 1986 *Phys. Scr.* **33** 192
[17] Strečka J 2006 *Physica* A **360** 379
[18] Jaščur M and Strečka J 2005 *Condensed Matter Phys.* **8** 869
[19] da Silva N R and Salinas S R 1991 *Phys. Rev.* B **44** 852
Albayrak E and Keskin M 2003 *J. Magn. Magn. Mater.* **261** 196
[20] Ekiz C 2005 *J. Magn. Magn. Mater.* **293** 759
[21] Oitmaa J 2005 *Phys. Rev.* B **72** 224404
[22] Albayrak E and Yilmaz S 2008 *Physica* A **387** 1173
Ekiz C 2008 *Physica* A **387** 1185
[23] Buendía G M and Machado E 1998 *Phys. Rev.* E **58** 1260
[24] Keskin M, Canko O and Polat Y 2008 *J. Korean Phys. Soc.* **53** 497
[25] Glauber R J 1963 *J. Math. Phys.* **4** 294
[26] Godoy M and Figueiredo W 2000 *Phys. Rev.* E **61** 218
[27] Godoy M and Figueiredo W 2002 *Phys. Rev.* E **65** 026111
[28] Godoy M and Figueiredo W 2002 *Phys. Rev.* E **66** 036131
[29] Godoy M and Figueiredo W 2004 *Braz. J. Phys.* **34** 422
Godoy M and Figueiredo W 2004 *Physica* A **339** 392
[30] Ekiz C and Keskin M 2003 *Physica* A **317** 517
[31] Albayrak E and Alçi A 2005 *Physica* A **345** 48
Ekiz C 2005 *J. Magn. Magn. Mater.* **293** 913
[32] Zhang X and Kong X M 2006 *Physica* A **369** 589
[33] Jaščur M and Strečka J 2005 *Physica* A **358** 393
[34] Strečka J and Čanová L 2006 *Condensed Matter Phys.* **9** 179
[35] Strečka J 2006 *Phys. Status Solidi* b **243** 708
[36] Albayrak E 2003 *Int. J. Mod. Phys.* B **17** 1087
Ekiz C 2006 *J Magn. Magn. Mater.* **307** 139
[37] Deviren B, Keskin M and Canko O 2009 *J. Magn. Magn. Mater.* **321** 458
[38] Keskin M, Kantar E and Canko O 2008 *Phys. Rev.* E **77** 051130
[39] Ekiz C 2005 *Physica* A **353** 286
[40] Maťašovská S and Jaščur M 2007 *Physica* A **383** 339
[41] Deviren B, Keskin M and Canko O 2009 *Physica* A **388** 1835
[42] Albayrak E and Yigit A 2007 *Phys. Status Solidi* b **244** 748
[43] Albayrak E and Yigit A 2006 *Phys. Lett.* A **353** 121
[44] Zhang Q, Wei G and Gu Y 2005 *Phys. Status Solidi* b **242** 924
[45] Keskin M, Ertaş M and Canko O 2009 *Phys. Scr.* **79** 025501
[46] Wei G Z, Gu Y W and Liu J 2006 *Phys. Rev.* B **74** 024422
Zhang Q, Wei G, Win Z and Lang Y 2004 *J. Magn. Magn. Mater.* **280** 14
[47] Albayrak E and Yigit A 2005 *Physica* A **349** 471
[48] Kaneyoshi T, Nakamura Y and Shin S 1998 *J. Phys.: Condens. Matter* **10** 7025
Nakamura Y 2000 *Phys. Rev.* B **62** 11742
[49] Wei G Z, Zhang Q and Xin Z H 2004 *J. Magn. Magn. Mater.* **277** 1
[50] Albayrak E and Yigit A 2007 *Physica* A **375** 174
[51] Honmura R and Kaneyoshi T 1979 *J. Phys. C: Solid State Phys.* **12** 3979
[52] Kaneyoshi T, Fittipaldi I P, Honmura R and Manabe T 1981 *Phys. Rev.* B **24** 481
[53] Balcerzak T 1991 *J. Magn. Magn. Mater.* **97** 152
[54] Kaneyoshi T and Beyer H 1980 *J. Phys. Soc. Japan* **49** 1306
[55] Hai T and Li Z Y 1989 *Phys. Status Solidi* b **156** 641
Hai T, Li Z Y, Lin G L and George T F 1991 *J. Magn. Magn. Mater.* **97** 227
[56] Jascur M and Kaneyoshi T 1993 *J. Phys.: Condens. Matter* **5** 6313
[57] Kaneyoshi T 1987 *J. Phys. Soc. Japan* **56** 2675
Kaneyoshi T 1988 *Physica* A **153** 556
Li Z Y and Kaneyoshi T 1988 *Phys. Rev.* B **37** 7785
Kaneyoshi T 1989 *Solid State Commun.* **70** 975
Kaneyoshi T 1990 *J. Magn. Magn. Mater.* **92** 59
Kaneyoshi T 1994 *Physica* A **205** 677
[58] Benayad N, Klumper A, Zittartz J and Benyoussef A 1989 *Z. Phys.* B **77** 339
[59] Bobák A and Jurčišin M 1997 *Physica* A **240** 647
[60] Callen H B 1963 *Phys. Lett.* **4** 161
[61] Kaneyoshi T, Jaščur M and Tomczak P 1992 *J. Phys.: Condens. Matter* **4** L653
Kaneyoshi T, Tucker J W and Jaščur M 1992 *Physica* A **186** 677
[62] Kaneyoshi T and Jaščur M 1993 *Phys. Status Solidi* b **175** 225
[63] Kaneyoshi T, Honmura R, Tamura I and Sarmento E F 1984 *Phys. Rev.* B **29** 5121
[64] Zernike F 1940 *Physica* A **7** 565
[65] Kaneyoshi T, Tamura I and Sarmento E F 1983 *Phys. Rev.* B **28** 6491
Kaneyoshi T 1986 *Phys. Rev.* B **33** 7688
[66] Kaneyoshi T, Jaščur M and Tomczak P 1993 *J. Phys.: Condens. Matter* **5** 5331
[67] Kaneyoshi T, Jaščur M and Fittipaldi I P 1993 *Phys. Rev.* B **48** 250
[68] Hui K 1988 *Phys. Rev.* B **38** 802
Keskin M, Pınar M A, Erdinç A and Canko O 2006 *Physica* A **364** 263
[69] Wei G Z, Liang Y Q, Zhang Q and Xin Z H 2004 *J. Magn. Magn. Mater.* **271** 246
[70] Jiang W and Bai B D 2006 *Phys. Status Solidi* b **243** 2892
[71] Balcerzak T 2003 *Physica* A **317** 213
Jiang W, Bai B D and Wei G Z 2005 *Physica* A **354** 301
Jiang W, Bai B D, Lo V C and Liu W 2005 *J. Appl. Phys.* **97** 10B307
Mancini F and Naddeo A 2006 *Phys. Rev.* E **74** 061108
Canpolat Y, Torgursul A and Polat H 2007 *Phys. Scr.* **76** 597
[72] Kaneyoshi T and Jaščur M 1992 *Phys. Rev.* B **46** 3374
Jiang W, Wie G Z and Xin Z H 2001 *Phys. Status Solidi* b **225** 215
Kaneyoshi T 2004 *Physica* A **339** 403
[73] Doerr M, Kramp S and Loewenhaupt M 2001 *Physica* B **294** 164
[74] Koyama K and Fujii H 2001 *Physica* B **294** 168
[75] Albertini F, Bolzoni F and Paoluzi A 2001 *Physica* B **294** 172